KeAi
CHINESE ROOTS
GLOBAL IMPACT

Available online at www.sciencedirect.com

ScienceDirect

Green Energy & Environment 7 (2022) 533–544

www.keaipublishing.com/gee

Research paper

Mechanistic study of vacuum UV catalytic oxidation for toluene degradation over CeO_2 nanorods

Muyan Wu [a], Yingguang Zhang [a], Haibao Huang [b,*], Dennis Y.C. Leung [a,*]

[a] Department of Mechanical Engineering, The University of Hong Kong, Pokfulam Road, Hong Kong, China
[b] School of Environmental Science and Engineering, Sun Yat-sen University, Guangzhou, 510275, China

Received 7 August 2020; revised 30 October 2020; accepted 11 November 2020
Available online 18 November 2020

Abstract

The present study specifically investigates vacuum ultraviolet (VUV) catalytic oxidation for toluene degradation over CeO_2 nanorods. Synergetic effects of ultraviolet photocatalytic oxidation (UV-PCO) and ozone catalytic oxidation (OZCO) were manifested in the results of toluene removal and COx generation, while the combination of UV-PCO and OZCO (UV-OZCO) did not lead to improvement of mineralization. All the processes contribute to ozone decomposition, but no obvious synergetic effects of the different processes can be observed. Intermediate analysis results indicated that more toluene was oxidized into by-products, such as benzyl alcohol and benzaldehyde, by UV-OZCO rather than forming COx. Both hydroxyl radical (·OH) and superoxide radical ($\cdot O_2^-$) were found in all the processes of the VUV-PCO-OZCO system (combination of VUV photolysis, UV-PCO, OZCO and UV-OZCO processes). In the UV-OZCO process, the formation of hydroxyl radical was promoted, while that of superoxide radical was impeded, resulting in lower mineralization level of toluene. The mechanistic study of toluene degradation over CeO_2 nanorods in the VUV-PCO-OZCO system revealed that with the formation of $\cdot O_2^-$ and ·OH, toluene is first oxidized to intermediates, followed by further ring–opening reaction and, finally, degradation into CO_2 and H_2O. CeO_2 nanorods function as both ozonation catalyst and photocatalyst, and the redox pair of Ce^{3+} and Ce^{4+} are interconvertible and can keep a balance.

Keywords: Vacuum ultraviolet; VOCs; Ozone; Photocatalysis; Catalytic ozonation

1. Introduction

Volatile organic compounds (VOCs) are getting increasing public attention due to their potential threat to human beings and the environment [1,2]. Therefore, many studies focused on technology development to eliminate VOCs have been reported. Among them, advanced oxidation processes (AOPs) are regarded as one of the most promising technologies due to their strong oxidation capacities and high efficiencies. Typical AOPs include catalytic oxidation [3,4], ozone catalytic oxidation [5,6] and photocatalytic oxidation [7,8]. Reactive species, such as hydroxyl radicals, superoxide radicals and atomic oxygen, can be generated in these processes. In order to further improve performance, more than one AOP were combined in one system for VOCs degradation [9–11].

In recent years, combined AOP system based on vacuum ultraviolet (VUV) irradiation was one of the topics that attracted the greatest attention; it involves multiple processes, including VUV photolysis, UV photocatalytic oxidation (UV-PCO), ozone catalytic oxidation (OZCO), as well as the combination of UV photocatalytic oxidation and ozone catalytic oxidation (UV-OZCO). VUV light is a type of ultraviolet light with wavelength of 185 nm and corresponding photon energy of 6.7 eV. Under VUV irradiation, VOCs can be degraded by direct bond breaking as well as oxidation by the reactive species generated, such as ozone, hydroxyl radical

* Corresponding authors.
E-mail addresses: huanghb6@sysu.edu.cn (H. Huang), ycleung@hku.hk (D.Y.C. Leung).

https://doi.org/10.1016/j.gee.2020.11.002

(·OH) and superoxide radical ($\cdot O_2^-$). In the presence of the generated ozone and UV light, ozone catalytic oxidation and photocatalytic oxidation as well as the combination of these two processes may occur when using specific catalysts. A great number of studies about combination of AOPs based on VUV irradiation have been reported. Ji et al. [12] applied mesoporous TiO_2 in photocatalytic oxidation enhanced by VUV irradiation for benzene degradation. Shu et al. [13] synthesized the composite Mn/TiO_2/activated carbon (AC) catalysts and applied it in a VUV ozone-assisted catalytic oxidation system, where high efficiencies of VOCs degradation and O_3 elimination can be achieved. Xu et al. [14] developed a VUV-PCO air purifier with nanoporous TiO_2 as photocatalyst and Mn-Fe composite as ozonation catalyst. The purifier was found to possess good activity in both VOC removal and O_3 decomposition in actual indoor environment. Huang et al. [15] combined the processes of VUV photolysis and ozone catalytic oxidation using Mn/ZSM-5 as catalysts. Benzene and O_3 could be completely removed, and the reaction pathways as well as mechanism of the combined system were proposed. Liang et al. [16] studied the degradation mechanism of toluene in a system combining VUV photolysis and photocatalytic oxidation by analyzing the by-products generated from the reaction of toluene oxidation. However, to the best of our knowledge, existing studies mainly focused on catalyst development and performance evaluation of the combined VUV system. Although some of the studies analyzed the pathways of the reaction system, only two or less than two processes based on VUV irradiation were involved in these studies.

Catalysts used in the VUV catalytic oxidation system need to possess both the functions of photocatalysis and catalytic ozonation. Most existing studies applied composite materials to realize simultaneous VOC degradation and ozone decomposition. In our previous work [17], pure CeO_2 was shown to possess the capacities of photocatalysis and catalytic ozonation, making it an excellent catalyst for the catalytic oxidation system. CeO_2 nanorods exhibited the best performance in toluene degradation and ozone elimination among all the synthetic CeO_2 samples.

As VUV catalytic oxidation is regarded as one of the most promising technologies in VOC degradation, efforts are being made to improve this technology for practical application in air pollution control. Understanding the reaction mechanisms is essential for catalyst development and system optimization of VUV catalytic oxidation. However, there are still no mechanistic studies involving all the processes, including VUV photolysis, UV-PCO, OZCO and UV-OZCO. The synergetic effects of these processes are also lacking in previous studies. In this study, we applied CeO_2 nanorods in the VUV catalytic oxidation system for toluene degradation involving all the processes of VUV photolysis, UV-PCO, OZCO and UV-OZCO. Mechanistic insights of the composite system were investigated by analyzing the by-products' formation, chemical properties of catalysts and radical generation in different processes. The synergetic effects of different processes and toluene degradation pathways are also proposed in this paper.

2. Experimental procedure

2.1. Synthesis of CeO_2 catalysts

CeO_2 nanorod samples were synthesized according to the method used in our previous study [17]: 3 g of $Ce(NO_3)_3 \cdot H_2O$ and 6.4 g of NaOH were dissolved in 30 mL and 50 mL of deionized (DI) water, respectively. After complete dissolution, the $Ce(NO_3)_3$ solution was added dropwise into the NaOH solution under vigorous stirring. The mixture was transferred to a Teflon reactor and placed in a stainless steel autoclave. After reaction at 100 °C for 14 h, the solid products were washed with DI water 4 times. After drying at 60 °C for 12 h, the yellow powders were calcined by a muffle oven at 400 °C for 4 h in air atmosphere.

2.2. Characterization of catalysts

The morphology and selected area electron diffraction (SAED) of the CeO_2 samples were observed by scanning transmission electron microscopy (STEM, FEI Tecnai G2 20 S-TWIN). X-ray diffraction (XRD) spectra were obtained by a Rigaku SmartLab 9 kW X-ray diffractometer with Cu Kα radiations at 45 kV and 200 mA. Electron Paramagnetic Resonance (EPR) test was conducted using a Bruker A300 spectrometer, and 5, 5-dimethyl-1-pyrroline N-oxide (DMPO) was used as the scavenger of hydroxyl radical (·OH) and superoxide radical ($\cdot O_2^-$). X-ray photoelectron spectroscopy (XPS) was used to analyze the chemical states of CeO_2 catalysts before and after usage by an X-ray photoelectron spectrometer (Thermo Fisher Scientific K-Alpha) using Al K radiation with an energy of 1486.8 eV.

2.3. Experimental set-up

The experimental set-up of toluene degradation by catalytic oxidation is shown in Fig. 1. Inlet gases containing toluene, water vapor, ozone and clean air were generated and mixed in the gas distributing system. Clean and dry air was first generated by a zero air generator and distributed into three, including toluene generation, water vapor generation and ozone generation, controlled by mass flow controllers. In the experiments of OZCO and UV-OZCO, ozone was generated by an ozone generator and adjusted to the same concentration level as ozone generated by the VUV lamps, while in other experiments, ozone generator was bypassed using two three-way valves. The inlet mixed air contained 30 ppm of toluene and 50% of relative humidity (optimum value indicated by a previous study [18]) with a total flow rate of 1.5 L min^{-1}. The mixed air then passed through the reaction system, and a stainless steel tank was used as the reactor with two 4 W VUV lamps installed inside for the experiments of VUV-photolysis and VUV-PCO-OZCO. In the experiments of UV-PCO and

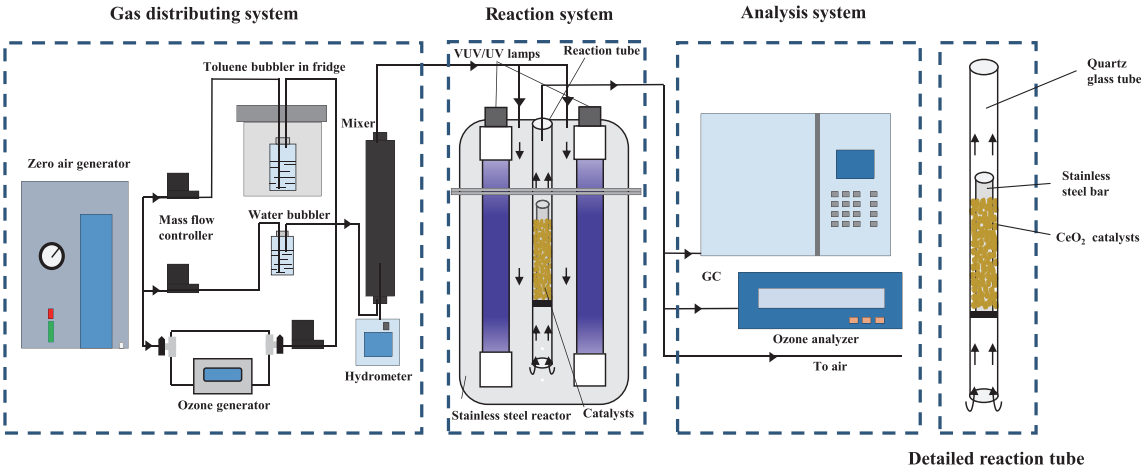

Fig. 1. Experimental set-up of toluene degradation by catalytic oxidation over CeO_2 catalysts.

UV-OZCO, two UV lamps with the same power and UV intensity of VUV lamps are fixed in the reactor instead, while in the experiment of OZCO, no lamps were installed in the reactor. One gram (1 g) of the synthetic CeO_2 samples were fixed in a quartz reaction tube with a stainless steel bar placed in the middle of the catalysts to enlarge the illumination area of the catalysts. The gas hourly space velocity (GHSV) was determined to be $1.2 \times 10^5\ h^{-1}$. After reaction, the outlet gas was analyzed in the analysis system. The concentrations of toluene were measured by a flame-ionization detector (FID) equipped in a gas chromatograph (GC, FULI, 9790PLUS) using an RB-TVOC (50 m * 0.32 mm) column, while the concentrations of CO and CO_2 were measured by an FID equipped with a TDX-01 (2 m * 3 mm) column. Outlet ozone was detected by an ozone analyzer (2B Technologies, Model 202). Intermediates in the toluene degradation reaction were detected by GC–MS (Shimadzu, GCMS-QP2010 SE).

Toluene removal efficiency, mineralization, COx generation rate as well as ozone removal rate are calculated by the following equations respectively [19]:

$$\text{Toluene removal efficiency}\,(\%) = \frac{[\text{Toluene}]_{\text{inlet}} - [\text{Toluene}]_{\text{outlet}}}{[\text{Toluene}]_{\text{inlet}}} \times 100\%$$

$$\text{Mineralization rate}\,(\%) = \frac{[\text{CO}]_{\text{generated}} + [\text{CO}_2]_{\text{generated}}}{[\text{Toluene}]_{\text{degraded}} \times 7} \times 100\%$$

$$[\text{COx}]_{\text{generated}} = [\text{CO}]_{\text{outlet}} - [\text{CO}]_{\text{inlet}} + [\text{CO}_2]_{\text{outlet}} - [\text{CO}_2]_{\text{inlet}}$$

$$\text{O}_3\ \text{removal rate}\,(\%) = \frac{[\text{O}_3]_{\text{generated}} - [\text{O}_3]_{\text{outlet}}}{[\text{O}_3]_{\text{generated}}} \times 100\%$$

3. Results and discussion

Fig. 2 shows the TEM images and XRD pattern of the synthetic CeO_2 nanorods. As displayed in Fig. 2(a), the synthetic CeO_2 exhibits nano-sized rod-shape with a width of 5–8 nm and a length of 18–40 nm respectively. Fig. 2(b) shows an HRTEM image of a single CeO_2 nanorod. According to the fast Fourier transform (FFT) pattern in the inset, lattice fringes with inter-planar spacing of 0.312 nm and 0.271 nm can be observed in the CeO_2 nanorod, which depict the presence of (111) and (200) planes, respectively. XRD was conducted to analyze the crystal structure of the synthetic CeO_2 nanorods as shown in Fig. 2(c). Eight peaks representing (111), (200), (220), (311), (222), (400), (331) and (420) were obtained; they are the characteristic peaks of fluorite structure (Fm3m, JCPDS 34–0394) of CeO_2. Clear rings can be observed in the selected-area electron diffraction (SAED) pattern (Fig. 2c inset) obtained by HRTEM, indicating the crystalline structure of the CeO_2 nanorods. The recognized crystal planes from SAED pattern are in great accordance with the XRD results. The BET results and UV-vis spectrum of the synthetic CeO_2 nanorods are shown in Figs. S1 and S2 in the supplementary data.

When applying VUV lights in catalytic oxidation system, four processes are involved, including VUV photolysis, UV photocatalytic oxidation (UV-PCO), ozone catalytic oxidation (OZCO) and UV assisted ozone catalytic oxidation (UV-OZCO). Combining all the above processes, the system can be termed VUV-PCO-OZCO. To have a deeper understanding of the mechanism, activity tests of the different processes in VUV based catalytic oxidation over CeO_2 nanorods were conducted. Toluene removal efficiencies, COx (CO and CO_2) generation, mineralization rates as well as ozone removal efficiencies of the different processes were evaluated to reveal the contributions and synergetic effects of these processes. Details of the testing conditions of the different processes are described in Section 2.3.

Time variation and average toluene removal efficiencies of the different processes are shown in Fig. 3. Toluene adsorption

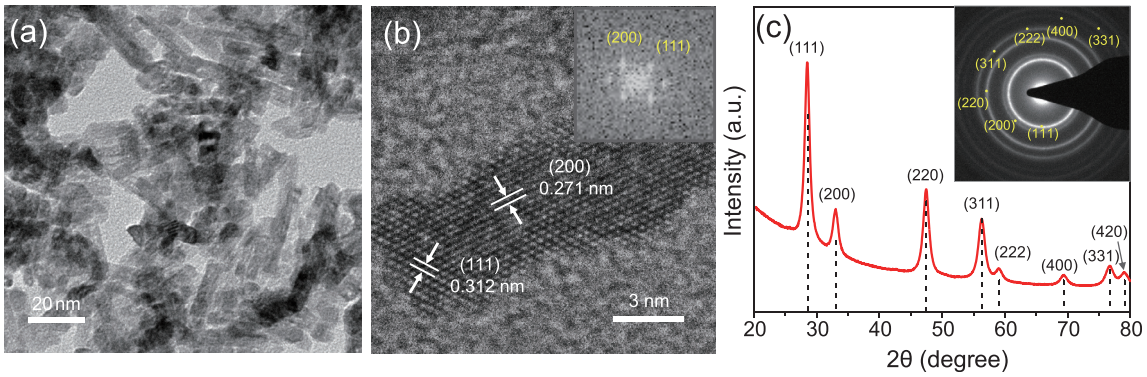

Fig. 2. (a) TEM image, (b) HRTEM image with fast Fourier transform (FFT) analysis pattern (inset) and (c) XRD spectrum with selected-area electron diffraction (SAED) pattern (inset) of CeO_2 nanorods.

effects were evaluated before the experiments, and the adsorption ability of the synthetic CeO_2 is negligible in the system. UV photolysis was estimated in preliminary experiments and results showed that the effect of UV photolysis on toluene was minimal. Thus, photolysis in the VUV catalytic oxidation system only refers to VUV photolysis in this study. All the toluene oxidation tests were repeated twice, and as shown in Fig. 3 (a), the excellent repeatability of the experiments is indicated by the minimal error bars. As displayed in Fig. 3, the toluene removal efficiencies of the different processes are ranked in the following order: VUV-PCO-OZCO > photolysis > UV-OZCO > OZCO > UV-PCO. The composite system involving all the processes possesses the best toluene degradation performance with an average toluene removal efficiency of 83.2% within the 144-min testing, while the contribution of UV-PCO is the least; its average toluene removal efficiency is only 2.4%. The VUV-PCO-OZCO system consists of the processes of photolysis and UV-OZCO. However, toluene removal efficiency follows the trend that photolysis + UV-OZCO > VUV-PCO-OZCO. The removal efficiencies of these processes were calculated based on the degraded toluene. However, in the VUV-PCO-OZCO system, toluene is first oxidized by the photolysis process, followed by further oxidation in the UV-OZCO process. A portion of the reactants in the UV-OZCO process is the by-products from the photolysis process rather than toluene. Therefore, the amount of organic compounds degraded in the VUV-PCO-OZCO system is larger than the removed toluene as recorded because the former also includes the intermediates from the photolysis process. This phenomenon will be further explained by the results of COx generation in Fig. 4. UV-OZCO contains the processes of UV-PCO and OZCO. The toluene removal efficiencies of these processes follow the rule that UV-PCO + OZCO < UV-OZCO, which indicates that synergetic effects exist between UV irradiation and ozone catalytic oxidation. The synergetic effects of these two processes are also manifested in the results of COx generation, O_3 removal and EPR.

To estimate the capacities of different processes to completely oxidize toluene into CO and CO_2, the concentrations of COx (CO + CO_2) generated from the different processes were measured, and the corresponding mineralization rates were determined. The results of mineralization and the average COx generation concentration of the different processes are shown in Fig. 4. As displayed in Fig. 4(a), the mineralization rates of the different processes are ranked in the following order: UV-PCO > VUV-PCO-OZCO ≈ OZCO > photolysis > UV-OZCO. UV-PCO exhibits the highest mineralization rate (71.1%

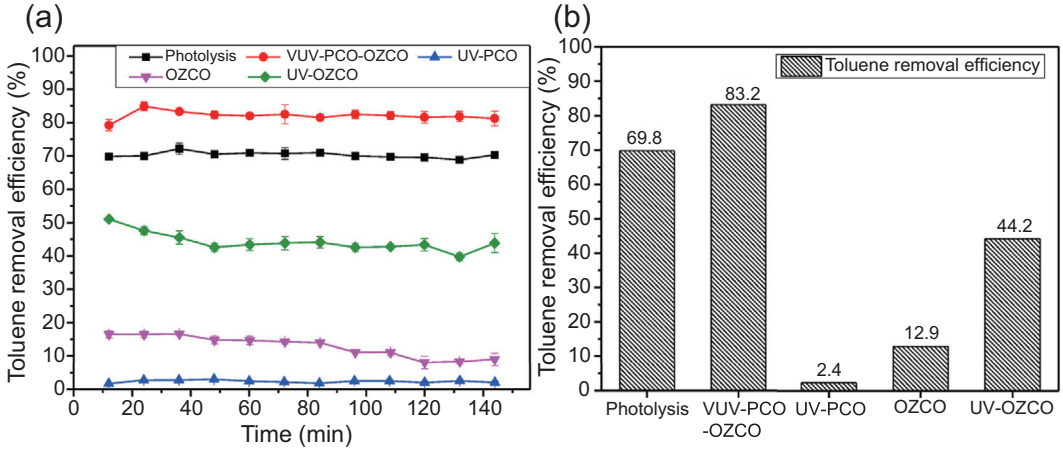

Fig. 3. (a) Time variation of toluene removal efficiencies and (b) average toluene removal efficiencies of different processes (Running conditions: Air flow: 1.5 L min^{-1}, RH: 50%, temperature: 25 °C, dose of catalysts: 1.0 g, GHSV: 1.2 × 10^5 h^{-1}, inlet toluene concentration: 30 ppm).

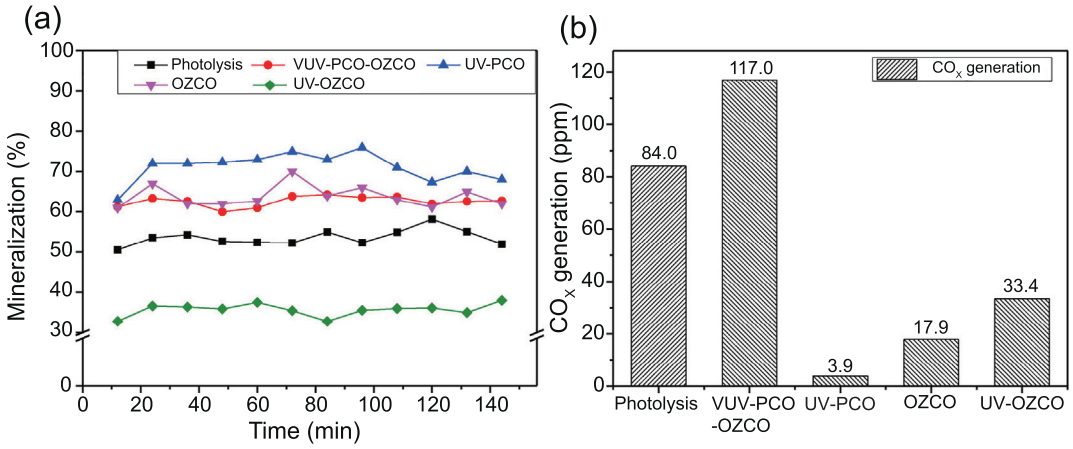

Fig. 4. (a) Mineralization and (b) average COx (CO + CO_2) generation of different processes (Running conditions same as those in Fig. 3).

on average), which indicates that the most thorough toluene degradation can be achieved by UV-PCO. Compared to pure photolysis, the average mineralization rate and COx generation concentration of VUV-PCO-OZCO increased from 53.6% to 62.6% and 84.0 ppm to 117.0 ppm respectively, which reveals that the introduction of CeO_2 nanorod catalysts can enhance complete toluene oxidation. VUV-PCO-OZCO and OZCO have similar mineralization capacities, with average mineralization rates of 62.6% and 63.8% respectively throughout the measurement period. Compared to OZCO and UV-PCO, UV-OZCO exhibits a decrement in mineralization, indicating that the combination of UV-PCO and OZCO cannot improve complete toluene oxidation, although higher toluene removal efficiency can be achieved by the combined process. As indicated in Fig. 4 b, COx generation by VUV photolysis, UV-OZCO and VUV-PCO-OZCO follow the trend that VUV photolysis + UV-OZCO ≈ VUV-PCO-OZCO. Combined with the toluene removal efficiency results, it is revealed that although the sum of the toluene removal efficiencies of photolysis and UV-OZCO is higher than the toluene removal efficiency of VUV-PCO-OZCO, the sum of the COx generated by the separate processes (photolysis + UV-OZCO) is approximately the same as the COx generated by the combined system (VUV-PCO-OZCO). The above phenomenon depicts that the combined system has a similar capacity of oxidizing toluene to COx compared with the sum of the separate processes of photolysis and UV-OZCO. The combination of photolysis and UV-OZCO does not lead to a more complete oxidation to COx of organic compounds. Thus, the process of photolysis mainly contributes to the preliminary oxidation of toluene rather than showing synergetic effect with the subsequent process of UV-OZCO. The concentration of the COx generated by UV-OZCO is higher than the sum of the COx generated by UV-PCO and OZCO, which further illustrates the synergy of UV irradiation and OZCO in the complete degradation of toluene.

In the presence of VUV lights, O_3 can be formed from oxygen decomposition, as elucidated by following the equations:

$$O_2 + h\nu(185\ \text{nm}) \rightarrow O(^1D) + O(^3P)$$

$$O(^1D) + O_2 \rightarrow O(^3P) + O_2$$

$$O(^3P) + O_2 \rightarrow O_3$$

In the VUV based catalytic oxidation system, the generated O_3 will be utilized for further toluene degradation by ozone catalytic oxidation. However, high concentration of residual ozone is detrimental to the environment and human bodies. Therefore, ozone removal efficiency is one of the essential indicators when evaluating the VUV catalytic oxidation system. This study estimated the ozone decomposition abilities of the different processes, and the results are shown in Fig. 5. The concentration of ozone generated from two 4W VUV lamps in the system was measured to be 107 ppm under an air flow of 1.5 L min^{-1}. Therefore, the concentration of ozone dosed into

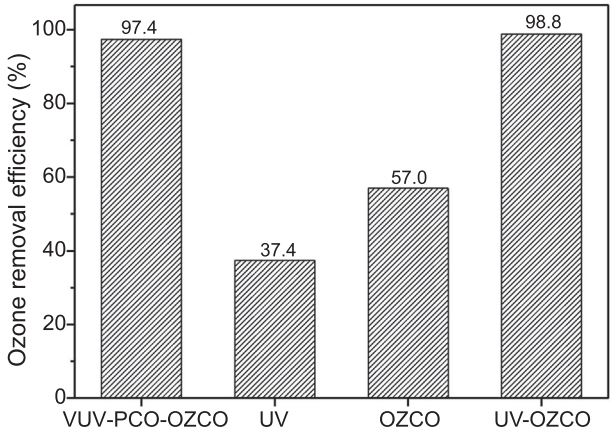

Fig. 5. Ozone removal efficiencies of different processes (Running conditions same as those in Fig. 3).

the system by the ozone generator was controlled to be 107 ppm using a mass flow controller when conducting the ozone decomposition tests of other processes. As indicated in Fig. 5, all the processes exhibit the ability of removing ozone to different extents. Thirty seven point four percent (37.4%) of ozone can be decomposed with only the irradiation of UV lights, which can be ascribed to the disruption of bonds in ozone molecules by UV light with wavelength of 240–300 nm [20]. In the presence of CeO_2 catalyst, 57.0% of ozone was removed in the process of ozone catalytic oxidation. The ozone removal efficiencies of the different processes follow the trend that VUV-PCO-OZCO ≈ UV-OZCO ≈ UV + OZCO, revealing that the effect of the composite process of UV and OZCO is similar to the addition of the separate processes. Thus, no obvious synergetic effects of the different processes were observed in ozone decomposition. Excellent capacities of ozone removal were obtained in VUV-PCO-OZCO and UV-OZCO, with ozone removal efficiencies of 97.4% and 98.8% respectively. Therefore, the adverse effects to the environment by the generated ozone can be reduced to a great extent.

For better understanding of the reaction pathways and the mechanisms of the different processes involved in the VUV catalytic oxidation system, intermediates from different processes of toluene degradation were detected by GC–MS. Both the intermediates of the gaseous phase from the outlet gas of the reaction system and the liquid phase adsorbed on the surface of catalysts were collected using methanol as the absorbent. The amounts of intermediates collected from the outlet gas were negligible and most of the intermediates were adsorbed on the catalyst surface, revealing that the toxicity of the outlet gas from the VUV catalytic oxidation system to the environment is minimal. Photolysis process refers to VUV photolysis as the effect of UV photolysis in toluene degradation was negligible according to some preliminary experiments. To collect the intermediates from the surface of the catalysts, 0.2 g of the used catalysts were immersed in 10 mL of methanol. After vigorous stirring and filtration, 1 μL of the solution was injected in GC–MS for detection. All the measurements of the intermediates collected from the used catalysts were obtained through the same treatment above. Thus, the relative quantities of intermediates on catalysts from the different processes can be obtained and compared. As displayed in Fig. 6, benzyl alcohol is the main intermediate and can be found in all the processes; it is formed by the oxidation of toluene by hydroxyl radical [21,22]. From further oxidation of benzyl alcohol, benzaldehyde is formed and can also be observed in all the processes. The relative amount of benzyl alcohol in the process of UV-OZCO is considerably higher than those in other processes, revealing that more toluene was oxidized into by-products rather than COx in UV-OZCO, which is in accordance with the results of mineralization in Fig. 4. There are two main pathways of toluene degradation: H atom abstraction from the methyl group of toluene and OH addition to the aromatic ring [21]. Apart from benzyl alcohol formed from H atom abstraction, 2-methylphenol (o-cresol)

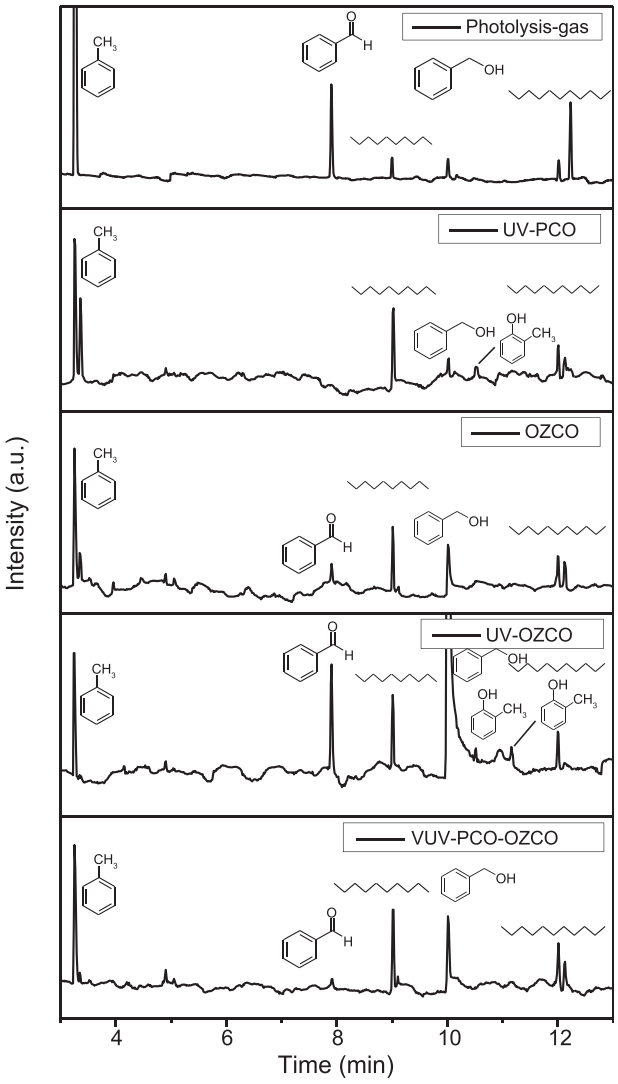

Fig. 6. Intermediates detected by GC–MS from different processes of toluene degradation.

can be obtained in the process of UV-PCO, while o-cresol and 3-methylphenol (m-cresol) can be obtained in UV-OZCO, indicating that OH addition to the aromatic ring happened in the two processes. According to previous results [23,24], the formation of m-cresol needs higher activation energy than o-cresol, while the branching ratio of o-cresol is much higher. Therefore, only with the combined effect of UV and OZCO processes can m-cresol be produced. Toxicities of the main intermediates in VUV catalytic oxidation system including benzyl alcohol, benzaldehyde, o-cresol and m-cresol are reported to be higher than the toxicity of toluene itself. However, as the gaseous intermediates in the outlet was negligible and the residual ozone can be greatly eliminated by pure CeO_2 catalyst, the toxicity of the treated outlet gas is limited to the environment.

To clarify the participation of CeO_2 catalysts, XPS tests were conducted to analyze the chemical changes of CeO_2 samples in the VUV catalytic oxidation system. The oxidation

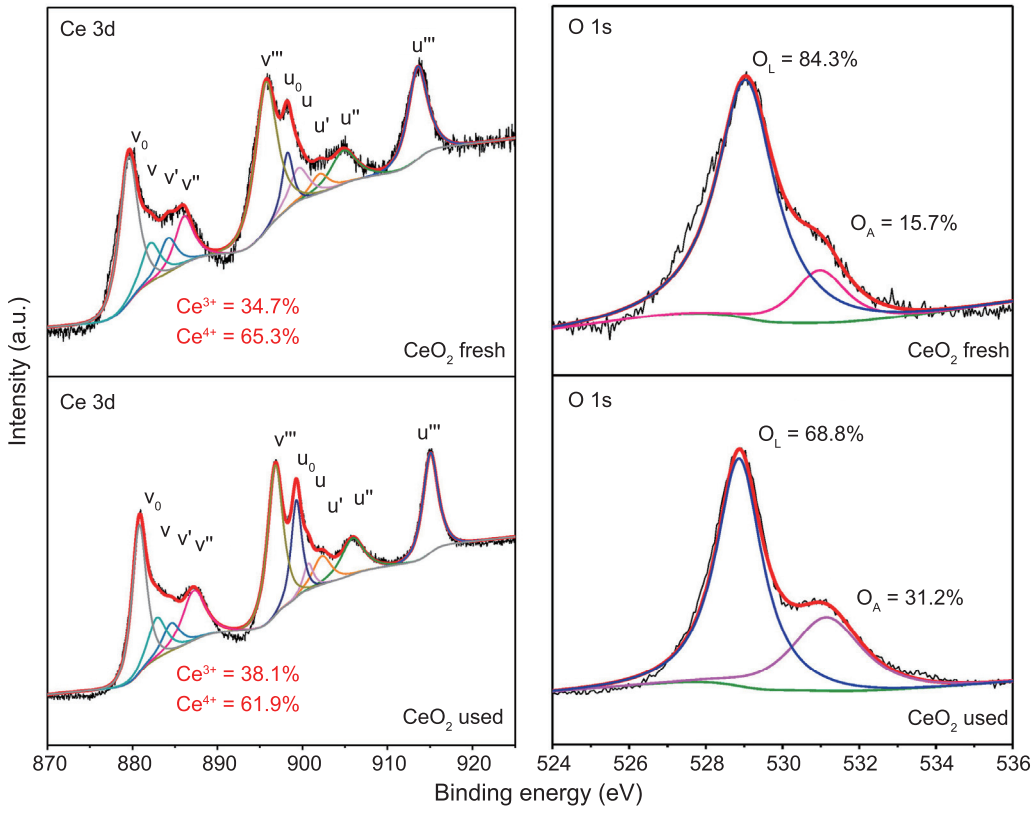

Fig. 7. XPS spectra of Ce 3d and O 1s of fresh and used CeO_2 samples.

states of both fresh CeO_2 sample and CeO_2 used in the VUV-PCO-OZCO system were investigated. As shown in Fig. 7, the Ce3d spectra of CeO_2 can be split into ten peaks including v_0 (880.8 eV), v (883.0 eV), v' (884.6 eV), v'' (887.3 eV), v''' (896.8 eV), u_0 (899.3 eV), u (900.7 eV), u' (902.4 eV), u''' (906.0 eV) and u''' (915.1 eV). The peaks of v, u, v'', u'', v''' and u''' are attributed to Ce^{4+}, while the peaks of v_0, u_0, v' and u' are characteristic of Ce^{3+}. The ratios of Ce^{3+} and Ce^{4+} can be calculated from the quotients of peak areas according to the following equations [17]:

$$Ce^{3+}(\%)=\frac{A_{v0}+A_{v'}+A_{u0}+A_{u'}}{A_{v0}+A_{v'}+A_{u0}+A_{u'}+A_{v}+A_{v''}+A_{v'''}+A_{u}+A_{u''}+A_{u'''}}\times 100\%$$

$$Ce^{4+}(\%)=\frac{A_{v}+A_{v''}+A_{v'''}+A_{u}+A_{u''}+A_{u'''}}{A_{v0}+A_{v'}+A_{u0}+A_{u'}+A_{v}+A_{v''}+A_{v'''}+A_{u}+A_{u''}+A_{u'''}}\times 100\%$$

The Ce^{3+} ratios of CeO_2 samples before and after use are calculated to be 34.7% and 38.1% respectively, while the Ce^{4+} ratios of the fresh and used samples are 65.3% and 69.1% respectively. The concentration of Ce^{3+} in the CeO_2 samples increased after use in the VUV-PCO-OZCO system. The transformation of the oxidation states of CeO_2 mainly happened in the process of ozone catalytic oxidation. Many studies have stated the importance of the redox pair of Ce^{3+}/Ce^{4+} in ozonation process [17,25]. A balance in the redox cycle of $Ce^{3+} \rightarrow Ce^{4+} \rightarrow Ce^{3+}$ can be achieved by the reactions between ozone and organic reactants. The introduced ozone can oxidize Ce^{3+} to Ce^{4+}, whereas Ce^{4+} is reduced to Ce^{3+} by organics adsorbed on the surface of CeO_2 catalysts through electron transfer process [26,27]. The increase of Ce^{3+} manifests the valence transformation of CeO_2 samples. The concentration of Ce^{3+} is crucial to the activity of CeO_2 catalysts, and no decline of Ce^{3+} concentration was observed, indicating that CeO_2 can remain active after use in the VUV-PCO-OZCO system throughout the study period.

The O 1s spectra of CeO_2 samples before and after use are also displayed in Fig. 7. The two peaks at 528.9 eV and 531.1 eV correspond to oxygen in the lattice structure (O_L) and oxygen adsorbed on the surface (O_A) respectively. By calculation of peak areas, the concentration of O_A in CeO_2 samples increased from 15.7% to 31.2% after use in the VUV-PCO-OZCO system, which could be ascribed to the formation of OH groups on the surface of the catalysts. It has been reported that OH groups participated in the adsorption of ozone and organic reactants, followed by subsequent degradations [25,26].

In order to confirm the stability and reusability of the CeO_2 catalysts in the VUV catalytic oxidation system, the toluene removal efficiencies and mineralization rates over CeO_2 in

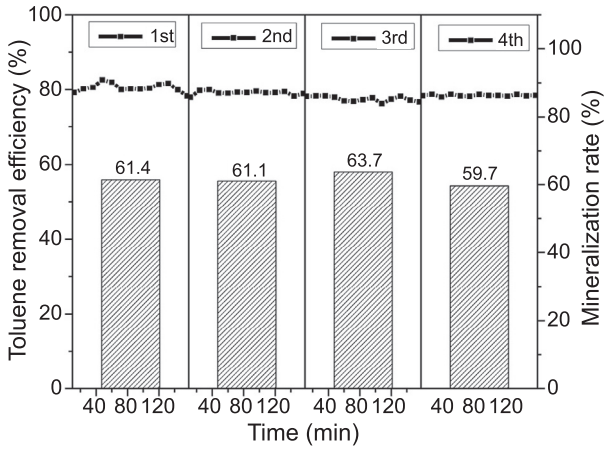

Fig. 8. Toluene removal efficiencies and mineralization rates of CeO_2 catalyst in repeated usages.

repeated usages were investigated. As shown in Fig. 8, the removal efficiencies of toluene over CeO_2 kept at ~80% in 4 cycles of reuse and no obvious decrease can been observed. Similarly, average mineralization rates of CeO_2 kept at 61%–64% during the 4 cycles. The above results manifest that the synthetic CeO_2 samples possess high stability and good reusability, which is consistent with the XPS results.

In advanced oxidation processes, the generation of reactive radicals that can oxidize organic reactants efficiently is essential. Hydroxyl radical (·OH) and superoxide radical ($\cdot O_2^-$) played a critical role in the oxidation processes of VUV-PCO-OZCO system. Hydrogen peroxide (H_2O_2) can also be formed in the presence of oxygen and electrons [28]. However, the generated H_2O can only be effectively utilized in the oxidation process through Fenton/Fenton-like reaction at a pH of 2.5–3.5 [29], which is not applicable in the present study. Therefore, investigation of hydrogen peroxide was not included. To analyze the effects and mechanisms of the different processes, EPR tests were carried out to validate the formation of ·OH and $\cdot O_2^-$ in these processes. DMPO was used as a scavenger to capture ·OH and $\cdot O_2^-$. During the test for hydroxyl radical, 100 mg of CeO_2 samples and 200 mL of DI water were added into a beaker. After ultrasonic dispersion, 100 μL of the solution was extracted, and 10 ppm of DMPO in water solution was added. The solution was drawn with a capillary pipette and put into a quartz NMR (nuclear magnetic resonance) tube to conduct the EPR tests. For the detection of $\cdot O_2^-$, the solvent was changed to methanol to avoid the interference of ·OH. In the process of EPR sample preparation, different treatments were applied to stimulate the reactions in different processes. To stimulate the process of VUV photolysis, no catalysts were introduced, and the solution with DMPO was irradiated with VUV lights together with the feeding of ozone (107 ppm). For the UV-PCO process, a solution with CeO_2 sample was irradiated with UV lights, and clean air with oxygen was fed into the solution. For OZCO stimulation, ozone (107 ppm) was fed into CeO_2 solution in the dark. For the UV-OZCO process, UV irradiation was applied and ozone (107 ppm) was fed simultaneously. In the VUV-PCO-OZCO process, a solution with CeO_2 samples was irradiated with VUV lights with the feeding of ozone (107 ppm).

Fig. 9(a) and (b) show the EPR spectra of hydroxyl and superoxide radicals in the different processes. The characteristic peaks of DMPO-·OH and DMPO-$\cdot O_2^-$ with diverse intensities can be observed in all the processes. Hydroxyl and superoxide radicals were generated in all the processes of VUV-PCO-OZCO system, while the relative amounts of ·OH and $\cdot O_2^-$ varied due to the different formation mechanisms. In the process of VUV-photolysis, the formation of hydroxyl and superoxide radicals mainly resulted from water photolysis and ozone decomposition when water and ozone are both present in the reactions as shown below [30–32]:

$$H_2O \xrightarrow{VUV} \cdot H + \cdot OH$$

$$O_3 \xrightarrow{UV} \cdot O + O_2$$

$$H_2O + \cdot O \rightarrow 2 \cdot OH$$

$$\cdot H + O_2 \rightarrow \cdot HO_2$$

$$\cdot HO_2 \rightarrow H^+ + \cdot O_2^-$$

In the UV-PCO process, the generation of ·OH and $\cdot O_2^-$ by CeO_2 catalysts is shown in the following equations:

$$CeO_2 + h\nu \rightarrow CeO_2\ (e^- + h^+)$$

$$h^+ + OH^- \rightarrow \cdot OH$$

$$O_2 + e^- \rightarrow \cdot O_2^-$$

As a semiconductor with a band gap of 3.2 eV, CeO_2 is considered a good photocatalyst [17,33,34]. With UV irradiation, the energy of photons will be absorbed by CeO_2, and an electron (e^-) will be excited from the valence band to the conduction band, resulting in the generation of an electron hole (h^+). The generated electron holes and electrons can react with hydroxyl group and oxygen to form hydroxyl and superoxide radicals respectively, which will participate in the subsequent oxidation of VOCs [35,36].

In the process of ozone catalytic oxidation, both hydroxyl and superoxide radicals can be generated in the toluene degradation reaction. Ozone can be easily adsorbed on the oxygen vacancy sites of CeO_2 (CeO_2-O_v) and decomposed into molecular oxygen and oxygen atom. In the presence of water, oxygen atoms will react with water vapor to form hydroxyl radical [17,19]. The generation of superoxide radical starts from the formation of ozonide (O_3^-) in the oxidation of Ce^{3+} to Ce^{4+}. O_3^- can then react with the O_4^{2-} formed in ozone

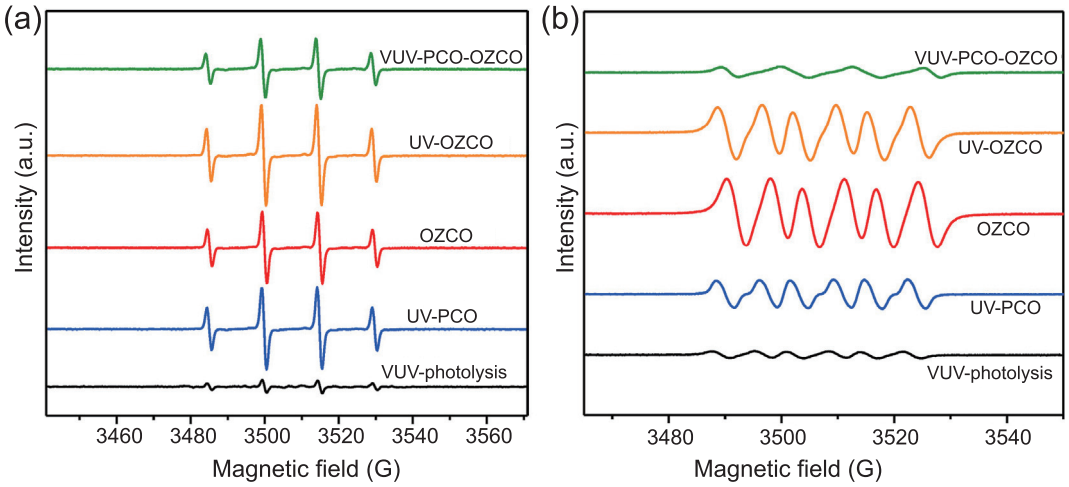

Fig. 9. EPR spectra of different processes: (a) spectra of DMPO-·OH (b) spectra of DMPO-·O_2^-

decomposition [37,38]. The corresponding reaction processes are shown below:

$$O_3 \xrightarrow{CeO_2-O_v} O_2 + O \quad (O_v = \text{oxygen vacancies})$$

$$O + H_2O \rightarrow 2\cdot OH$$

$$Ce^{3+} + O_3 \rightarrow Ce^{4+} + O_3^-$$

$$O_3 + O^{2-} \rightarrow O_4^{2-}$$

$$O_4^{2-} + O_3 \rightarrow O_4^- + O_3^- \rightarrow O_2 + \cdot O_2^- + \cdot O_3^-$$

As indicated by the EPR results in Fig. 9, the generation of hydroxyl radical in the combined process of UV photocatalysis and ozone catalytic oxidation (UV-OZCO) increased compared with OZCO or UV-PCO alone, while the formation of superoxide radical exhibited a slight decrease. The increase in hydroxyl radical formation and decline in superoxide radical formation are due to the participation of O_3, as discussed in other studies [39–41]. The relative reactions are shown below:

$$CeO_2 + h\nu \rightarrow CeO_2\ (e^- + h^+)$$

$$h^+ + OH^- \rightarrow \cdot OH$$

$$O_3 + e^- \rightarrow \cdot O_3^-$$

$$H^+ + \cdot O_3^- \rightarrow \cdot HO_3$$

$$\cdot HO_3 \rightarrow O_2 + \cdot OH$$

$$O_3 + h\nu \rightarrow \cdot O + O_2$$

$$\cdot O + H_2O \rightarrow 2\cdot OH$$

Compared to UV photocatalysis, O_3 acts as an electron acceptor to form ·OH instead of ·O_2^-. Furthermore, the decomposition of ozone by UV irradiation also results in the generation of ·OH. Therefore, in the UV-OZCO process, the formation of hydroxyl radicals was promoted, while that of superoxide radicals was impeded.

In VUV-PCO-OZCO, the formation of hydroxyl and superoxide radicals exhibit an obvious decline compared to other processes, which can be ascribed to the fact that under the irradiation of light with wavelength shorter than 250 nm, DMPO can absorb the light, and carbon-centered DMPO adducts can be formed, which results in the consumption of DMPO [42]. Thus, lower amounts of DMPO-·OH and DMPO-·O_2^- can be detected.

To further confirm the effects of ·OH and ·O_2^- radicals in the VUV catalytic oxidation system, toluene removal efficiency and mineralization rates over CeO_2 treated with different radical scavengers were measured. 10 mmol L^{-1} of tert-butanal (TBA) and 1 mmol L^{-1} of benzoquinone (BQ) were used as scavengers to captured ·OH and ·O_2^- radicals, respectively. As displayed in Fig. 10(a), average toluene removal efficiencies decreased from 82.1% over non-treated CeO_2 to 72.3% and 77.0% over CeO_2 treated by TBA and BQ, respectively. Toluene removal efficiency of TBA-treated catalyst decreased more compared to BQ-treated catalyst, indicating that hydroxyl radicals exhibited greater effects in toluene degradation in the VUV catalytic oxidation system. Mineralization of scavenger-treated CeO_2 was also investigated and results are shown in Fig. 10(b). Compared to non-treated CeO_2, the average mineralization rate in 144 min of TBA-treated catalyst decreased slightly from 62.6% to 61.3%, whereas that of BQ-treated CeO_2 decreased more to 57.0%. The results of mineralization manifested that superoxide radicals played a more significant role in mineralization of toluene than hydroxyl radicals. The above results confirmed the generation of hydroxyl radicals and superoxide radicals, which possess important contributions

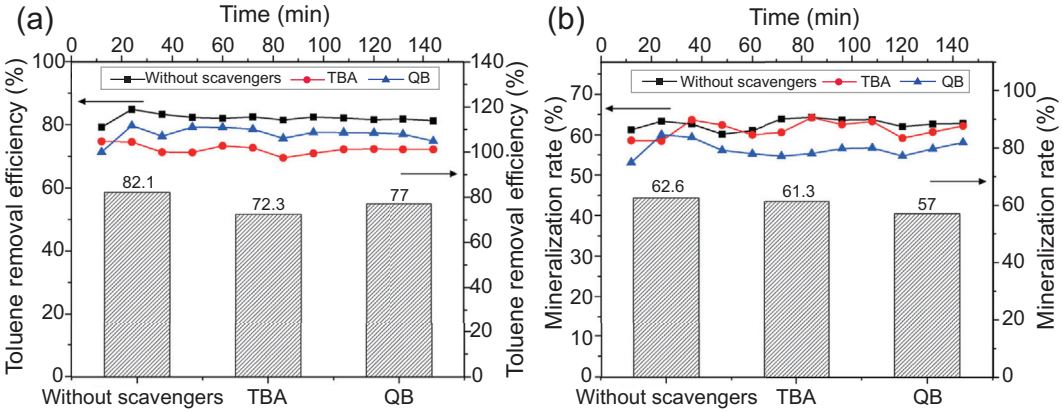

Fig. 10. Toluene removal efficiency (a) and mineralization rates (b) of CeO_2 treated by different scavengers.

to different extents in toluene degradation through the VUV catalytic oxidation.

According to the characteristics of the by-products detected and confirmation of radical generation, possible pathways of toluene degradation in the different processes of VUV based catalytic oxidation were proposed. The reaction pathways of the four separate processes are shown in Fig. 11, and the pathway of the combined VUV-PCO-OZCO system include all the separate oxidation pathways. The oxidation of toluene mainly originates from two routes: the abstraction of H atom in the methyl group of toluene and the direct addition of OH to benzene ring. In the process of VUV photolysis, without the participation of catalysts, the H atom in the methyl group can be easily abstracted by VUV irradiation forming benzyl radical [22], while in OZCO process, the H atom abstraction is mainly due to the reaction with OH radical. In both UV-PCO and UV-OZCO, where UV irradiation is involved, H atom can be abstracted by two routes, including direct hole transfer and H atom abstraction by hydroxyl radical [43]. The generated benzyl radical from these processes can react with oxygen to form tetroxide, which can be easily decomposed into benzyl alcohol and benzaldehyde based on the Russel reaction [21]. In the processes of UV-PCO and UV-OZCO, the direct addition of OH to benzene ring can also be observed, leading to the formation of o-cresol and m-cresol. All the products above will be further oxidized, and superoxide radical plays a critical role in the ring opening reaction of benzene rings [44]. Therefore, a lower generation of $\cdot O_2^-$ in the process of UV-OZCO may result in a lower mineralization rate, although it has a relatively high efficiency of toluene removal.

Based on all the above results, the mechanism of toluene degradation in VUV catalytic oxidation system is proposed and summarized in Fig. 12. With the application of VUV lamps that irradiate light at both 185 nm and 254 nm, O_3 can be generated from oxygen, while with the effect of irradiation or with CeO_2 catalyst, $\cdot O_2^-$ and $\cdot OH$ can be formed in the presence of water molecules. CeO_2 participates as the ozonation catalyst in this process. The redox pair of Ce^{3+} and Ce^{4+} is interconvertible and can keep a balance by the reaction of ozone oxidation and toluene electron transfer. Meanwhile,

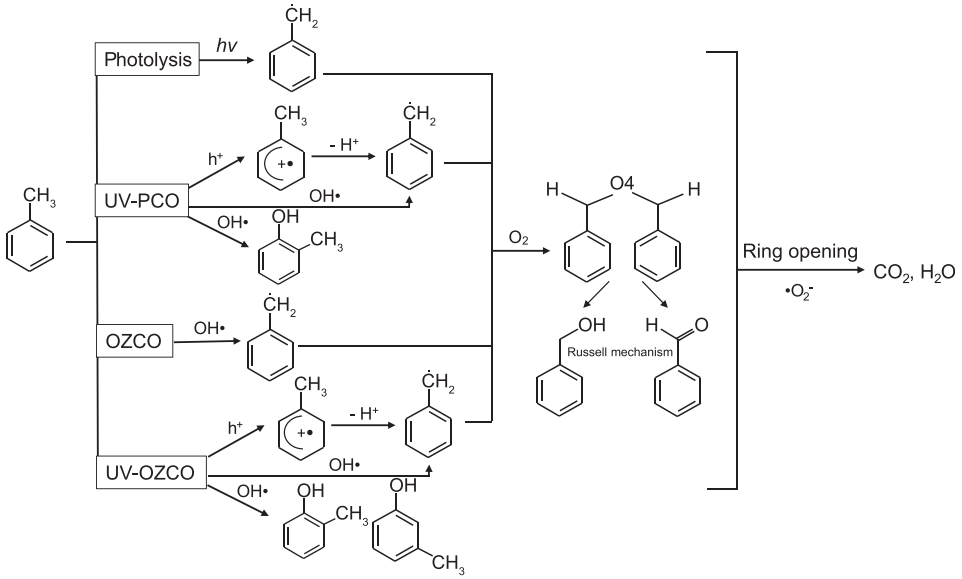

Fig. 11. Proposed pathways of toluene degradation in different processes of VUV based catalytic oxidation.

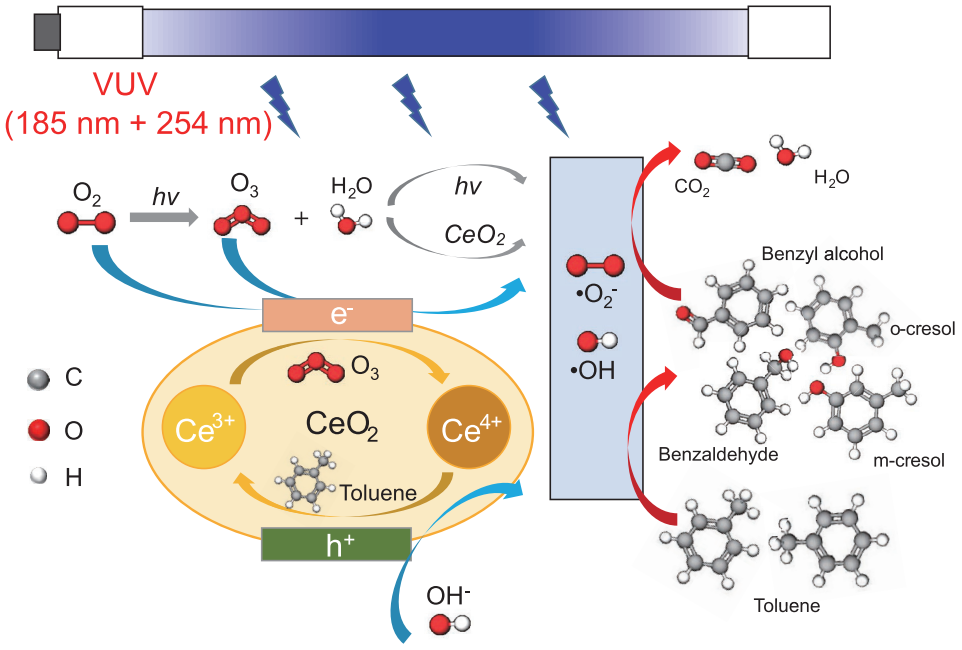

Fig. 12. Proposed mechanism of toluene degradation over CeO_2 in VUV-PCO-OZCO system.

CeO_2 also plays the role of photocatalysts, where electrons (e^-) and holes (h^+) are formed under the irradiation of UV light. Both O_2 and O_3 can be electron acceptors, while OH^- can be combined with holes. Furthermore, both $\cdot O_2^-$ and $\cdot OH$ are also formed in this process. With the generated radicals, toluene is first oxidized to intermediates, including benzyl alcohol, benzaldehyde, o-cresol and m-cresol, followed by further ring–opening reaction and final degradation into CO_2 and H_2O.

4. Conclusions

CeO_2 nanorods were applied in a VUV-PCO-OZCO system, involving VUV-photolysis, UV-PCO, OZCO and UV-OZCO processes. Toluene removal efficiency and COx generation follow the trend of UV-PCO + OZCO < UV-OZCO, indicating that synergetic effect exists between UV-PCO and OZCO. However, the decline of mineralization in UV-OZCO revealed that the combination of UV-PCO and OZCO did not improve complete toluene oxidation. For ozone decomposition, all the processes exhibit the ability of removing ozone, and no obvious synergetic effects of the different processes was observed in removing ozone. The GC–MS results indicated that more toluene was oxidized into by-products in UV-OZCO. Both hydroxyl and superoxide radicals were generated in all the processes of VUV-PCO-OZCO system. In the UV-OZCO process, the formation of hydroxyl radical was promoted, while that of superoxide radical was impeded. Superoxide radical plays a critical role in the benzene ring opening reaction; thus, a lower generation of $\cdot O_2^-$ in the process of UV-OZCO will result in a lower level of mineralization. The mechanism of toluene degradation over CeO_2 in VUV-PCO-OZCO system was summarized. $\cdot O_2^-$ and $\cdot OH$ can be formed with the participation of O_3, H_2O and CeO_2 catalysts. CeO_2 plays the role of both ozonation catalyst and photocatalyst, and the redox pair of Ce^{3+} and Ce^{4+} is interconvertible and can keep a balance. With the generated radicals, toluene can be first oxidized to intermediates, followed by further ring–opening reaction and final degradation into CO_2 and H_2O.

Under the same power, VUV lights have a shorter wavelength with stronger energy, which exhibits a much better performance in VOCs degradation compared to UV light. Therefore, VUV catalytic oxidation is more cost-effective than UV photocatalysis. As compared to ozone catalytic oxidation process, using VUV light can greatly improve the efficiencies from 12.9% to 83.2% with the catalyst as indicated in this study. Thus, VUV catalytic oxidation is also more effective than ozone catalytic oxidation.

Conflict of interest

The authors declare that they have no known competing financial interests or personal relationships that could have appeared to influence the work reported in this paper.

Acknowledgement

The authors gratefully acknowledge the financial supports from the National Natural Science Foundation of China (NSFC) and The Research Grants Council (RGC) of Hong Kong Joint Research Scheme (No. 51561165015, No. N_HKU718/15).

Appendix A. Supplementary data

Supplementary data to this article can be found online at https://doi.org/10.1016/j.gee.2020.11.002.

References

[1] J. Kong, Z. Xiang, G. Li, T. An, Appl. Catal. B Environ. 269 (2020) 118755.
[2] X. Wang, M. Sun, M. Murugananthan, Y. Zhang, L. Zhang, Appl. Catal. B Environ. 260 (2020) 118205.
[3] M.S. Kamal, S.A. Razzak, M.M. Hossain, Atmos. Environ. 140 (2016) 117–134.
[4] J. Zhao, W. Xi, C. Tu, Q. Dai, X. Wang, Appl. Catal. B Environ. 263 (2020) 118237.
[5] D. Xia, W. Xu, Y. Wang, J. Yang, Y. Huang, L. Hu, C. He, D. Shu, D.Y. Leung, Z. Pang, Environ. Sci. Technol. 52 (2018) 13399–13409.
[6] G. Chen, Z. Wang, F. Lin, Z. Zhang, H. Yu, B. Yan, Z. Wang, J. Hazard. Mater. 391 (2020) 122218.
[7] D. Xia, L. Hu, Y. Wang, B. Xu, Y. Liao, C. He, L. Ye, X. Liang, Y. Ye, D. Shu, Appl. Catal. B Environ. 256 (2019) 117811.
[8] H. Zhou, Z. Wen, J. Liu, J. Ke, X. Duan, S. Wang, Appl. Catal. B Environ. 242 (2019) 76–84.
[9] G. Liu, J. Ji, H. Huang, R. Xie, Q. Feng, Y. Shu, Y. Zhan, R. Fang, M. He, S. Liu, Chem. Eng. J. 324 (2017) 44–50.
[10] R. Xie, J. Ji, K. Guo, D. Lei, Q. Fan, D.Y. Leung, H. Huang, Chem. Eng. J. 356 (2019) 632–640.
[11] F. Zhang, B. Hong, W. Zhao, Y. Yang, J. Bao, C. Gao, S. Sun, Chem. Commun. 55 (2019) 3757–3760.
[12] J. Ji, Y. Xu, H. Huang, M. He, S. Liu, G. Liu, R. Xie, Q. Feng, Y. Shu, Y. Zhan, Chem. Eng. J. 327 (2017) 490–499.
[13] Y. Shu, Y. Xu, H. Huang, J. Ji, S. Liang, M. Wu, D.Y. Leung, Chemosphere 208 (2018) 550–558.
[14] T. Xu, H. Zheng, P. Zhang, Build. Environ. 142 (2018) 379–387.
[15] H. Huang, H. Huang, Y. Zhan, G. Liu, X. Wang, H. Lu, L. Xiao, Q. Feng, D.Y. Leung, Appl. Catal. B Environ. 186 (2016) 62–68.
[16] S. Liang, Y. Shu, K. Li, J. Ji, H. Huang, J. Deng, D.Y. Leung, M. Wu, Y. Zhang, J. Hazard. Mater. 399 (2020) 122967.
[17] M. Wu, Y. Zhang, W. Szeto, W. Pan, H. Huang, D.Y. Leung, Chem. Eng. Sci. 200 (2019) 203–213.
[18] H. Huang, H. Huang, L. Zhang, P. Hu, X. Ye, D.Y. Leung, Chem. Eng. J. 259 (2015) 534–541.
[19] M. Wu, D.Y. Leung, Y. Zhang, H. Huang, R. Xie, W. Szeto, F. Li, Chem. Eng. Sci. 195 (2019) 985–994.
[20] A.M. Mihalatos, A.C. Calokerinos, Anal. Chim. Acta 303 (1995) 127–135.
[21] J. van Durme, J. Dewulf, W. Sysmans, C. Leys, H. van Langenhove, Chemosphere 68 (2007) 1821–1829.
[22] Y. Shu, M. He, J. Ji, H. Huang, S. Liu, D.Y. Leung, J. Hazard. Mater. 364 (2019) 770–779.
[23] I. Suh, D. Zhang, R. Zhang, L.T. Molina, M.J. Molina, Chem. Phys. Lett. 364 (2002) 454–462.
[24] Y. Ji, J. Zhao, H. Terazono, K. Misawa, N.P. Levitt, Y. Li, Y. Lin, J. Peng, Y. Wang, L. Duan, Proc. Natl. Acad. Sci. U.S.A. 114 (2017) 8169–8174.
[25] S. Afzal, X. Quan, S. Lu, Appl. Catal. B Environ. 248 (2019) 526–537.
[26] B. Legube, N.K.V. Leitner, Catal. Today 53 (1999) 61–72.
[27] M.P. da Silva, L. Soeira, K. Daghastanli, T. Martins, I. Cuccovia, R. Freire, P. Isolani, J. Therm. Anal. Calorim. 102 (2010) 907–913.
[28] A. Torres-Pinto, M.J. Sampaio, C.G. Silva, J.L. Faria, A.M. Silva, Appl. Catal. B Environ. 252 (2019) 128–137.
[29] O. Osegueda, A. Dafinov, J. Llorca, F. Medina, J. Sueiras, Chem. Eng. J. 262 (2015) 344–355.
[30] S. Na, C. Jinhua, M. Cui, J. Khim, Ultrason. Sonochem. 19 (2012) 1094–1098.
[31] L. Yang, Z. Liu, J. Shi, Y. Zhang, H. Hu, W. Shangguan, Separ. Purif. Technol. 54 (2007) 204–211.
[32] B.H.J. Bielski, in: L. Packer (Ed.), Methods in Enzymology, Elsevier B.V., Amsterdam, 1984, pp. 81–88.
[33] H. Ren, P. Koshy, W.-F. Chen, S. Qi, C.C. Sorrell, J. Hazard. Mater. 325 (2017) 340–366.
[34] D. Channei, B. Inceesungvorn, N. Wetchakun, S. Ukritnukun, A. Nattestad, J. Chen, S. Phanichphant, Sci. Rep. 4 (2014) 5757.
[35] S. Banerjee, S.C. Pillai, P. Falaras, K.E. O'shea, J.A. Byrne, D.D. Dionysiou, J. Phys. Chem. Lett. 5 (2014) 2543–2554.
[36] B.M. da Costa Filho, G.V. Silva, R.A. Boaventura, M.M. Dias, J.C. Lopes, V.J. Vilar, Sci. Total Environ. 687 (2019) 1357–1368.
[37] K. Bulanin, J. Lavalley, J. Lamotte, L. Mariey, N. Tsyganenko, A. Tsyganenko, J. Phys. Chem. B 102 (1998) 6809–6816.
[38] M. Zhang, B. Jin, Y. Liu, W. Liu, D. Weng, X. Wu, S. Liu, Chem. Eng. J. 375 (2019) 121961.
[39] J. Xiao, Y. Xie, H. Cao, Y. Wang, Z. Zhao, Catal. Commun. 66 (2015) 10–14.
[40] X. Huang, J. Yuan, J. Shi, W. Shangguan, J. Hazard. Mater. 171 (2009) 827–832.
[41] P. Zhang, F. Liang, G. Yu, Q. Chen, W. Zhu, J. Photochem. Photobiol. Chem. 156 (2003) 189–194.
[42] C.F. Chignell, A.G. Motten, R.H. Sik, C.E. Parker, K. Reszka, Photochem. Photobiol. 59 (1994) 5–11.
[43] O. D'hennezel, P. Pichat, D.F. Ollis, J. Photochem. Photobiol. Chem. 118 (1998) 197–204.
[44] M. Sleiman, P. Conchon, C. Ferronato, J.-M. Chovelon, Appl. Catal. B Environ. 86 (2009) 159–165.